THE CONCEPT OF SCALE-CHANGING NETWORK IN THE GLOBAL ELECTROMAGNETIC SIMULATION OF COMPLEX STRUCTURES

H. Aubert [†]

CNRS, LAAS
7 avenue du colonel Roche, Toulouse F-31077, France

Abstract—The concept of Scale-Changing Network is reported for the electromagnetic modeling of complex planar structures composed of a collection of metallic patterns printed on a dielectric surface and whose size covers a large range of scale. Examples of such multi-scale structures are provided by multi-band frequency-selective surfaces, finite-size arrays of non-identical cells and fractal planar objects. Scale-Changing Networks model the electromagnetic coupling between various scale levels in the studied structure and are computed separately. The cascade of Scale-Changing Networks bridges the gap between the smallest and the highest scale levels and allows forming a monolithic (unique) electromagnetic formulation for the global electromagnetic simulation of complex planar structures. Derivation of these networks is presented and key advantages of the electromagnetic approach are reported.

1. INTRODUCTION

Nowadays global electromagnetic simulators are indispensable for accurate predictions of the overall electromagnetic performances of radiofrequency systems. When it involves both large structures (in terms of wavelength) and fine details the system or structure is said *complex*. The higher the number of scale levels the higher complexity. Well-known examples of complex structures are provided by multi-band frequency-selective surfaces, finite-size arrays of non-identical cells and fractal planar objects. The present paper is focused on the electromagnetic simulation of a generic multi-scale structure consisting

---

Corresponding author: H. Aubert (aubert@laas.fr).

[†] H. Aubert is also with Université de Toulouse, UPS, INSA, INP, ISAE, LAAS, Toulouse F-31077, France

of a collection of metallic patterns printed on a dielectric planar surface and whose size covers a large range of scale.

The electromagnetic simulation of multi-scale structures by meshing-based techniques (e.g., Finite Element Method, Finite Difference Time-Domain method or Transmission Line Matrix method) requires prohibitive execution time and memory resources. The numerical techniques based on spectral discretization (e.g., Mode Matching Technique, Integral Equation-Method developed in the spectral domain) share the same numerical limitations but, in addition, provide densely populated matrices with poor condition number and suffer from numerical convergence problems when applying to multi-scale structures. Recently, promising improvements of the Method of Moments have been proposed for reducing the execution time and memory storage for large-scale structures — see, e.g., the impedance matrix localization, the pre-corrected Fast Fourier Transform, the Fast Multipole Method and the Generalized Sparse Matrix Reduction Technique. However the convergence of numerical results remains delicate to reach systematically for non-expert users. The *Characteristic Basis Method of Moment* has been proposed for solving numerical problems generated by the electromagnetic simulation of multi-scale objects [1, 2] but, the construction of *Characteristic Basis Functions* for expanding the unknown current on such objects may be very time consuming and may require in practice large memory storage capabilities. Finally the electromagnetic simulation of multi-scale structures may also be performed by the combination or *hybridization* of various numerical techniques, each technique being the most appropriate for each particular scale level. However such coupling between heterogeneous formulations or the interconnection of various simulation tools is very delicate in practice.

In order to overcome the above-mentioned theoretical and practical difficulties, an original monolithic (unique) formulation for the electromagnetic modelling of multi-scale planar structures has been proposed by the author and his collaborators. This new technique consists of interconnecting *Scale-Changing Networks*, each network models the electromagnetic coupling between adjacent scale levels. The cascade of Scale Changing Networks allows the global electromagnetic simulation of multi-scale structures, from the smallest to the highest scale. Multi-modal sources, called *Scale-Changing Sources,* are artificially incorporated at all scale levels for the derivation of the network. When the complex surface presents both large regions and fine details — but no structures at intermediary scale levels-, mono-modal sources are able to model the electromagnetic coupling between the disparate scale levels [3–5]. However, for objects involving

multiple structures whose size covers a large range of scale, mono-modal sources fail to provide accurate numerical results while the Scale-Changing Sources allow the modelling of the scale crossing from the smallest to the highest scale (the number of modes in these sources can be derived from numerical convergence criteria). The global electromagnetic simulation of multi-scale structures via the cascade of *Scale Changing Networks* has been applied with success to the design and electromagnetic simulation of specific planar structures such as reconfigurable phase-shifters [6, 7], multi-frequency selective surfaces [8], discrete self-similar (pre-fractal) scatterers [9, 10] and patch antennas [11, 12]. This Scale-Changing technique is a very fast technique and this makes it a very powerful investigation, design and optimization tool for engineers who design complex circuits (see, e.g., [13–15]). Because of space limitations, the theory behind the proposed technique has never been fully described in our previous papers, where a particular attention was devoted to specific and attractive applications. The present paper provides the reader detailed theory on the key concept of Scale-Changing Network. The derivation of the Scale-Changing Network is presented in the framework of a generic planar multi-scale structure composed of a collection of metallic patterns printed on a dielectric surface and whose size covers a large range of scale.

The paper is organized as follows: The concept of Scale-Changing Network is introduced in Section 2. In the framework of Scale-Changing approach passive and active modes are defined and, the Scale-Changing Network is derived from the resolution of a specific boundary value problem involving *Scale-Changing Sources*. The Scale-Changing Sources are defined as intermediary sources that are artificially introduced for the non-redundant computation of the Scale-Changing Networks. The Section 3 is devoted to the *Scale-Changing Technique*, i.e., to the electromagnetic modelling of complex (multi-scale) planar structures via the interconnection of appropriate Scale-Changing Networks. The features of the proposed approach are summarized. The perspectives foreseen for this work are finally reported in Section 4.

2. THE SCALE-CHANGING NETWORK

Consider multiple metallic patterns printed on a dielectric surface and whose size covers a large range of scale. Suppose that many decades separate the largest pattern to the smallest one. This complex discontinuity plane may be positioned in a waveguide or located in free-space. At both sides of the plane the half-regions are composed of

multilayered and lossless dielectric media.

2.1. Partitioning of Complex Discontinuity Plane

The starting point of the proposed approach consists of the coarse partitioning of the complex discontinuity plane into large sub-domains of comparable sizes and arbitrary shape (step 1); in each sub-domain a second partitioning is performed by introducing smaller sub-domains of comparable sizes (step 2); Again, in each sub-domain introduced at the previous step a third partitioning is performed by introducing smaller sub-domains (step 3); and so on, as illustrated on Figure 1.
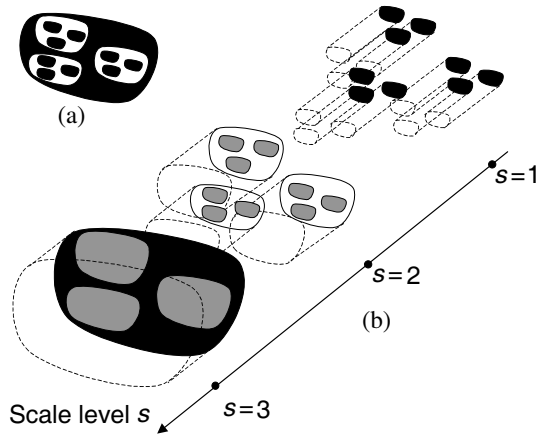
Figure 1. (a) An example of discontinuity plane presenting 3 scale-levels (black is metal and white is dielectric) and (b) the scattered view of the various sub-domains generated by the partitioning process.

Such hierarchical domain-decomposition allows focusing rapidly on increasing detail in the discontinuity plane. It is stopped when the finest dimension — or smallest scale — is reached. To each sub-domain is associated a scale-level: In particular, to the largest sub-domains corresponds conventionally the scale level $s = s_{\max}$ while, the scale level $s = 1$ corresponds to the smallest sub-domains.

For the sake of clarity the Figure 2 sketches the scattered views of the various subdomains generated by the partitioning process recently applied to some particular discontinuity planes.

As illustrated in Figure 3, suppose that the partitioning process applied at scale level s to the generic domain $D_i^{(s)}$ (where i designates an integer taken between 1 and I_s) generates J_{s-1} sub-domains $D_j^{(s-1)}$ (with $j = 1, 2, \ldots, J_{s-1}$). For example in case of Figure 2(c) the

adopted partitioning implies $J_2 = 4$ at scale level $s = 3$ and $J_1 = 4$ at scale level $s = 2$. In addition to the sub-domains $D_j^{(s-1)}$ the generic domain $D_i^{(s)}$ is assumed to be composed of perfect electric conductors and lossless dielectric regions.

Along the J_{s-1} contours $C_j^{(s-1)}$ of sub-domains $D_j^{(s-1)}$ and along the contour $C_j^{(s)}$ of the larger domain $D_i^{(s)}$ artificial boundary
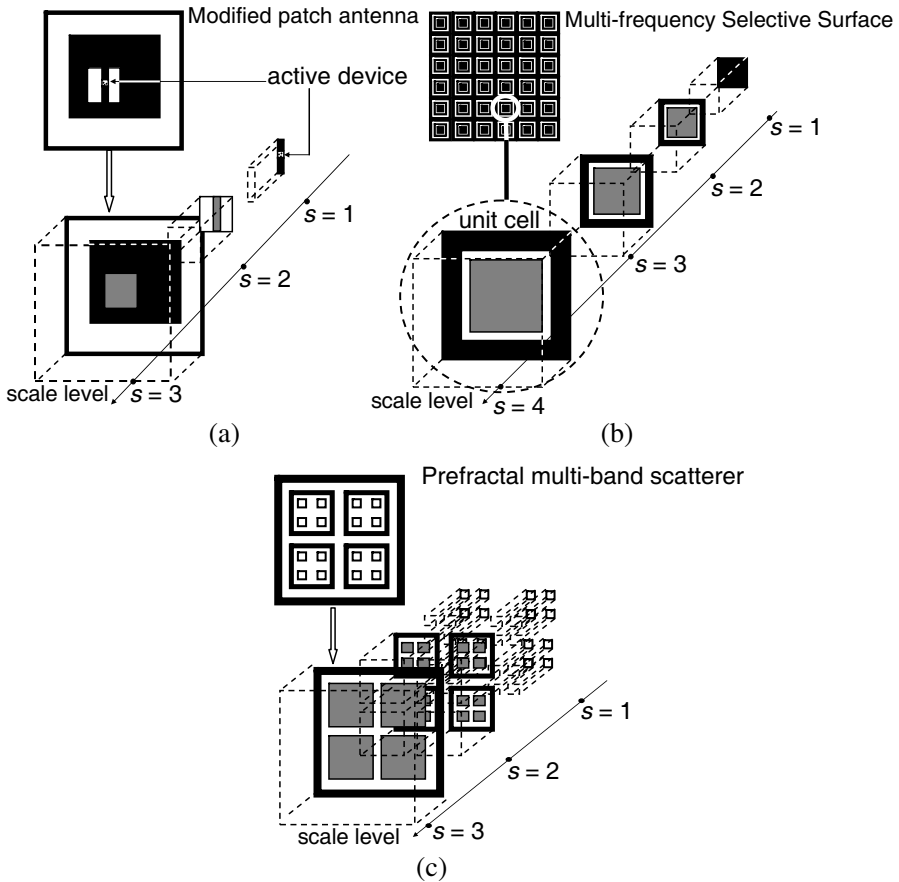
Figure 2. Some recently studied discontinuity planes and the scattered view of the various sub-domains generated by the partitioning process. (a) Modified patch antenna [11, 12], (b) multi-frequency selective surface [8], and (c) discrete self-similar (pre-fractal) scatterer [9, 10].
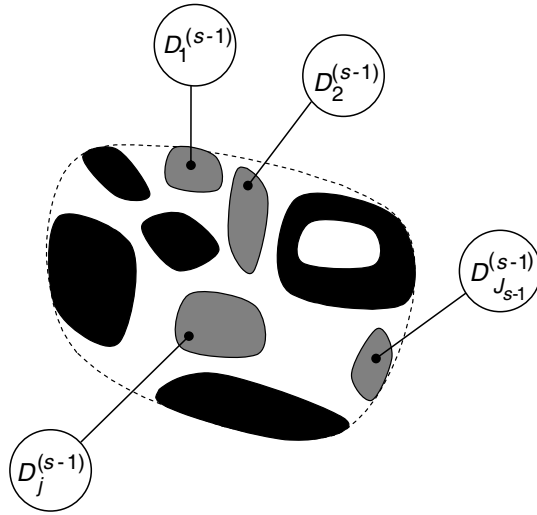
Figure 3. The i-th generic domain $D_i^{(s)}$ resulting from the partition process at scale level s black is perfect electric conductor, white is lossless dielectric and grey indicates sub-domain $D_j^{(s-1)}$, with $j = 1, 2, \ldots, J_{s-1}$).

conditions are incorporated: Such conditions are prescribed only on the contours of the sub-domains, not in the two half regions located on both sides of these sub-domains. The physics of the problem may be useful in the choice of these conditions in order to avoid perturbation of the actual electromagnetic field when incorporating these artificial conditions. Along the contours the choice can be: (1) Perfect Electric Conducting (PEC) condition, (2) Perfect Magnetic Conducting (PMC) condition, (3) a succession of PEC and PMC conditions or else (4) Periodic Boundary Conditions. In practice boundary conditions have to be *tried* on the contour of each sub-domain and the quality of the numerical solution — in terms of accuracy, execution time, numerical convergence — has to be checked subsequently.

In the sub-domain $D_i^{(s)}$ enclosed by artificial boundary conditions the modal expansion of the tangential electromagnetic field can be performed. The nth mode $\vec{F}_n^{(i,s)}$ in $D_i^{(s)}$ is solution of the following Helmholtz equation [16]

$$\left[\nabla_T^2 + k_n^{(i,s)^2}\right] \vec{F}_n^{(i,s)} = \vec{0} \tag{1}$$

where ∇_T^2 denotes the two-dimensional (or Transverse) Laplacian

operator and $k_n^{(i,s)}$ the cut-off wave-number of the nth mode in $D_i^{(s)}$. Moreover $\vec{F}_n^{(i,s)}$ satisfies the specified (and artificial) boundary conditions along the contour $C_i^{(s)}$. The discrete set of modes $\left\{ \vec{F}_n^{(i,s)} \right\}_{n=1,2,\ldots}$ in the bounded sub-domain $D_i^{(s)}$ is normal that is, for $i = 1, 2, \ldots, I_s$:

$$\left\langle \vec{F}_m^{(i,s)}, \vec{F}_n^{(i,s)} \right\rangle = \iint\limits_{D_i^{(s)}} \left[\vec{F}_m^{(i,s)} \right]^* \cdot \vec{F}_n^{(i,s)} ds = 0 \text{ if } m \neq n \qquad (2)$$

where $\left[\vec{F}_m^{(i,s)} \right]^*$ designates the complex conjugate value of vector $\vec{F}_m^{(i,s)}$. In this paper a normalized set of mode $\left\{ \vec{F}_n^{(i,s)} \right\}_{n=1,2,\ldots}$ is used, thus that is, $\left\langle \vec{F}_m^{(i,s)}, \vec{F}_n^{(i,s)} \right\rangle = \delta_{mn}$ where δ_{mn} designates the Kronecker delta ($\delta_{mn} = 1$ if $m = n$, 0 otherwise).

2.2. Definition of Passive and Active Modes

Without calculations it can be anticipated that the tangential electromagnetic field in the generic sub-domain $D_i^{(s)}$ shown in Figure 3 contains smooth (large-scale) variations and highly irregular (fine-scale) fluctuations. The fine-scale variations can be described as the linear combination of an infinite number of higher-order modes in $D_i^{(s)}$. This combination of higher-order modes is spatially localized in the vicinity of discontinuities, sharp edges and various contours $C_j^{(s-1)}$ and consequently, it is not significantly involved in the description of the electromagnetic coupling between the various sub-domains $D_j^{(s-1)}$. For this reason, the higher-order modes that are incorporated in this linear combination are called *passive modes*. The large-scale contribution to the field in the domain $D_i^{(s)}$ is due to the electromagnetic coupling between the constitutive sub-domains $D_j^{(s-1)}$. These couplings can be modelled as the combination of only a limited number of lower-order modes and this contribution to the tangential electromagnetic field in $D_i^{(s)}$ is then localized in the modal (spectral) domain. Because they are involved in the description of the electromagnetic coupling between the various sub-domains $D_j^{(s-1)}$ included in $D_i^{(s)}$, these lower-order modes are called *active* modes. Finally, due to their largely different spatial frequencies, any active mode in $D_i^{(s)}$ weakly interacts

with any passive mode taken in the constitutive sub-domains $D_j^{(s-1)}$. It follows from these above-mentioned physical considerations that the electromagnetic coupling between the scale level s and the lower scale level $s-1$ can be modelled by describing how any active mode in the domain $D_i^{(s)}$ interacts with the active modes in sub-domains $D_j^{(s-1)}$.

Remark: Note that the above-defined active and passive modes differ from well-known *accessible* and *localized* modes introduced several years ago in the framework of modal analysis of interacting discontinuities in waveguides [17, 18]: While cascading discontinuities along a waveguide structure, only a limited number of (evanescent and propagating) modes participate in the electromagnetic coupling between adjacent discontinuities, the remaining (highly evanescent) modes being localized at the neighbourhood of each discontinuity; each highly evanescent mode — as well as the combination of these modes — is then spatially localized. These physical considerations are not applicable here as the multiple metallic patterns (or scatterers) that constitute the multi-scale structure are printed of the same surface and share the same discontinuity plane. In other words they are not distributed along an imaginary axis. Moreover, in the domain $D_i^{(s)}$ any passive mode is not localized in the vicinity of the contours $C_j^{(s-1)}$ but oscillates everywhere on the surface $D_i^{(s)}$ with a high spatial frequency: consequently, contrarily to the modal analysis of interacting discontinuities in waveguides, it cannot be argued a priori that this mode is not involved in the coupling between the sub-domains $D_j^{(s-1)}$. However, as discussed above, it can be claimed that *the combination of all passive modes* is spatially localized in the vicinity of the sub-domains $D_j^{(s-1)}$ and does not explore the rest of the discontinuity plane.

2.3. The Concept of the Scale-Changing Network

Following the physical considerations of Section 2.2 the electromagnetic coupling between the scale s and scale $s-1$ can be modelled by describing the electromagnetic interaction of any active mode in the domain $D_i^{(s)}$ with the active modes in sub-domains $D_j^{(s-1)}$ with $j = 1, 2, \ldots, J_{s-1}$. A convenient model for describing the coupling between these adjacent scale levels is provided by the multi-port of Figure 4. In this representation, one port corresponds to one active mode. This multi-port allows to relate the field at scale s (i.e., in $D_i^{(s)}$) to the field at smaller scale $s-1$ [i.e., in all sub-domains $D_j^{(s-1)}$ ($j = 1, 2, \ldots, J_{s-1}$)]. For this reason this multi-port is called the *Scale-Changing Network*
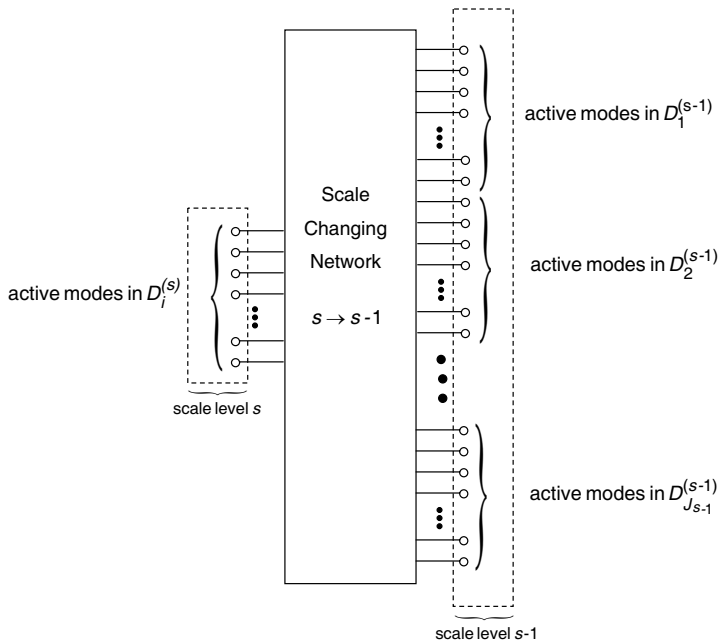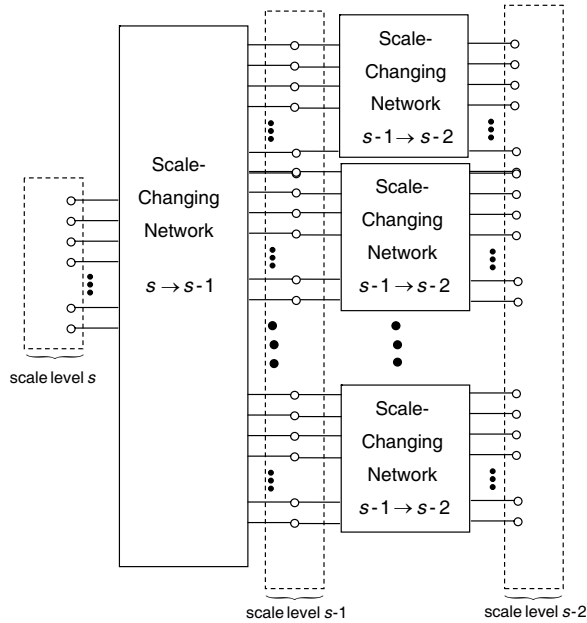
Figure 4. The Scale Changing Network coupling the active modes in the domain $D_i^{(s)}$ (scale level s) and its constitutive sub-domains $D_j^{(s-1)}$ (scale level $s-1$).

(SCN).

For relating the electromagnetic field at scale s to one at scale $s-2$, the interconnection of SCN may be performed as shown in Figure 5, each network being previously computed separately. Consequently, the modelling of interaction among the multiple scales in a complex discontinuity plane can be performed by cascading appropriate SCNs, each SCN models the electromagnetic coupling between two adjacent scale levels.

The cascading of SCN allows to relate the electromagnetic field between non adjacent scale levels and thus, modelling accurately the interaction among large-sized and small-sized parts of the structure. The SCN-based approach consists of:

(1) Partitioning the multi-scale structures under study into smaller and smaller sub-domains and by doing so, defining various scale levels such that two adjacent levels differ by one (or two) decade (s) [see Section 2.1];

(2) Computing separately the SCN describing the electromagnetic

Figure 5. The Scale-Changing Network that allows to relate the transverse electromagnetic field at scale s to one at scale $s - 2$.

    coupling between adjacent scales [see Section 2.5];

(3) Cascading all these SCNs to form a hierarchical graph for the modelling of the complete multi-scale structure.

    The derivation of the SCN's characteristic matrix requires the definition of artificial electromagnetic sources named the *Scale-Changing Sources* in the various sub-domains obtained from the partitioning process. The following Section defines these sources.

2.4. Definition of the Scale-Changing Sources

The derivation of the SCN that couples the scale s to the adjacent scale $s-1$ requires the resolution of a boundary value problem in which active modes act as actual sources named the modal *Scale Changing Sources*. When cascading the SCN for the global simulation of the multi-scale discontinuity plane, the two half regions on both sides of this plane has to be taken into accountonce. In order to formulate a non redundant approach the SCN computation incorporates the two half-regions at larger scale s only (and not at the smaller scale $s - 1$). It follows that the modal *Scale Changing Sources* at scale s differs from those at the

smaller scale $s - 1$.

2.4.1. Modal Scale-Changing Sources at the Larger Scale

At both sides of the generic sub-domain $D_i^{(s)}$ shown in Figure 3 the half-regions are composed of multilayered and lossless dielectric media. Throughout the paper these half-regions are denoted by the capital letters A and B, respectively. For $\alpha = A, B$ let $D_\alpha^{(i,s)}$ be the plane located in the half-region α and positioned infinitely close to the domain $D_i^{(s)}$; in addition let $\vec{n}^\alpha$ be the unit vector normal to $D_\alpha^{(i,s)}$ and oriented toward the half-region α; and finally, let $\vec{E}_\alpha^{(i,s)}$ and $\vec{H}_\alpha^{(i,s)}$ be respectively the tangential electric and magnetic fields on the domain $D_\alpha^{(i,s)}$. The set $\left\{ \vec{F}_n^{(i,s)} \right\}_{n=1,2,\ldots}$ of modes introduced in Section 2.1 is now used for the expansion of the tangential electromagnetic fields inside $D_A^{(i,s)}$ and $D_B^{(i,s)}$, that is:

$$
\begin{cases}
\vec{E}_\alpha^{(i,s)} = \sum\limits_{n=1}^{\infty} V_n^{(i,s,\alpha)} \vec{F}_n^{(i,s)} \\
\vec{J}_\alpha^{(i,s)} = \vec{H}_\alpha^{(i,s)} \times \vec{n}_\alpha = \sum\limits_{n=1}^{\infty} I_n^{(i,s,\alpha)} \vec{F}_n^{(i,s)}
\end{cases}
\quad \text{with } \alpha = A, B \qquad (3)
$$

where $V_n^{(i,s,\alpha)}$ and $I_n^{(i,s,\alpha)}$ denote respectively, the voltage and current amplitudes of the n-th mode in $D_\alpha^{(i,s)}$. Following the physical considerations of Section 2.2, the tangential electric field $\vec{E}_\alpha^{(i,s)}$ and the current density $\vec{J}_\alpha^{(i,s)} = \vec{H}_\alpha^{(i,s)} \times \vec{n}_\alpha$ in $D_\alpha^{(i,s)}$ may be written as follows:

$$
\begin{cases}
\vec{E}_\alpha^{(i,s)} = \vec{E}_\alpha^{(i,s)} \Big|_{large} + \vec{E}_\alpha^{(i,s)} \Big|_{fine} \\
\vec{J}_\alpha^{(i,s)} = \vec{J}_\alpha^{(i,s)} \Big|_{large} + \vec{J}_\alpha^{(i,s)} \Big|_{fine}
\end{cases}
\qquad (4)
$$

with

$$
\begin{cases}
\vec{E}_\alpha^{(i,s)} \Big|_{large} = \sum\limits_{n=1}^{N_\alpha^{(i,s)}} V_n^{(i,s,\alpha)} \vec{F}_n^{(i,s)} \text{ and } \vec{E}_\alpha^{(i,s)} \Big|_{fine} = \sum\limits_{n=N_\alpha^{(i,s)}+1}^{\infty} V_n^{(i,s,\alpha)} \vec{F}_n^{(i,s)} \\
\vec{J}_\alpha^{(i,s)} \Big|_{large} = \sum\limits_{n=1}^{N_\alpha^{(i,s)}} I_n^{(i,s,\alpha)} \vec{F}_n^{(i,s)} \text{ and } \vec{J}_\alpha^{(i,s)} \Big|_{fine} = \sum\limits_{n=N_\alpha^{(i,s)}+1}^{\infty} I_n^{(i,s,\alpha)} \vec{F}_n^{(i,s)}
\end{cases}
\qquad (5)
$$

where $N_\alpha^{(i,s)}$ denotes the number of active (propagating and evanescent) modes in the waveguide of cross-section $D_\alpha^{(i,s)}$. Since they

are highly evanescent in the artificial half-waveguide α (with $\alpha = A, B$), passive modes may be shunted by the purely reactive modal admittance $Y_n^{(i,s,\alpha)}$ viewed by $D_\alpha^{(i,s)}$. The analytical and generic expression of the modal admittance $Y_n^{(i,s,\alpha)}$ in case of multilayered dielectric structure located may be found in [19]. Consequently:

$$I_n^{(i,s,\alpha)} \approx Y_n^{(i,s,\alpha)} V_n^{(i,s,\alpha)} \text{ for } n > N_\alpha^{(i,s)} \tag{6}$$

From Eqs. (5) and (6) it can be deduced that

$$\vec{J}_\alpha^{(i,s)} \approx J_\alpha^{(i,s)}\Big|_{large} + \sum_{n=N_\alpha^{(i,s)}+1}^{\infty} Y_n^{(i,s,\alpha)} V_n^{(i,s,\alpha)} \vec{F}_n^{(i,s)} \tag{7}$$

This expression may be formally written as followed:

$$\vec{J}_\alpha^{(i,s)} = \vec{J}_\alpha^{(i,s)}\Big|_{large} + \hat{Y}_\alpha^{(i,s)} \vec{E}_\alpha^{(i,s)}$$

$$\text{with} \quad \hat{Y}_\alpha^{(i,s)} = \sum_{n=N_\alpha^{(i,s)}+1}^{\infty} \left| \vec{F}_n^{(i,s)} \right\rangle Y_n^{(i,s,\alpha)} \left\langle \vec{F}_n^{(i,s)} \right| \tag{8}$$

where $\hat{Y}_\alpha^{(i,s)}$ is an admittance operator. Note that only the passive modes in the half-waveguide α (with $\alpha = A, B$) are involved in $\hat{Y}_\alpha^{(i,s)}$. Following (5) the boundary conditions on the domain $D_i^{(s)}$ [that is, $\vec{E}_i^{(s)} = \vec{E}_A^{(i,s)} = \vec{E}_B^{(i,s)}$] becomes:

$$\sum_{n=1}^{\infty} V_n^{(i,s)} \vec{F}_n^{(i,s)} = \sum_{n=1}^{\infty} V_n^{(i,s,A)} \vec{F}_n^{(i,s)} = \sum_{n=1}^{\infty} V_n^{(i,s,B)} \vec{F}_n^{(i,s)}$$

$$\Rightarrow V_n^{(i,s)} = V_n^{(i,s,A)} = V_n^{(i,s,B)} \tag{9}$$

where $V_n^{(i,s)}$ denotes the voltage amplitude of the nth mode in $D_i^{(s)}$. Moreover, following Eq. (8), the current density $\vec{J}_i^{(s)} = \vec{J}_A^{(i,s)} + \vec{J}_B^{(i,s)}$ in $D_i^{(s)}$ becomes:

$$\vec{J}_i^{(s)} = \vec{J}_i^{(s)}\Big|_{large} + \hat{Y}_i^{(s)} \vec{E}_i^{(s)} \tag{10}$$

where

$$\begin{cases} \vec{J}_i^{(s)}\Big|_{large} = \sum_{\alpha=A,B} \vec{J}_\alpha^{(i,s)}\Big|_{large} = \sum_{n=1}^{N_A^{(i,s)}} I_n^{(i,s,A)} \vec{F}_n^{(i,s)} + \sum_{n=1}^{N_B^{(i,s)}} I_n^{(i,s,B)} \vec{F}_n^{(i,s)} \\ \hat{Y}_i^{(s)} = \hat{Y}_A^{(i,s)} + \hat{Y}_B^{(i,s)} = \sum_{\alpha=A,B} \sum_{n=N_\alpha^{(i,s)}+1}^{\infty} \left| \vec{F}_n^{(i,s)} \right\rangle Y_n^{(i,s,\alpha)} \left\langle \vec{F}_n^{(i,s)} \right| \end{cases} \tag{11}$$

For the sake of simplification in the theoretical developments the number of active modes in domains $D_A^{(i,s)}$ and $D_B^{(i,s)}$ may be taken identical, that is, $N_A^{(i,s)} = N_B^{(i,s)} = N^{(i,s)}$ where $N^{(i,s)}$ refers to *the number of active modes in the domain* $D_i^{(s)}$. The current *Scale Changing Sources* at scale s (domain $D_i^{(s)}$) are then defined by Eq. (10) with:

$$\begin{cases} \left. \vec{J}_i^{(s)} \right|_{large} = \sum_{n=1}^{N_i^{(s)}} I_n^{(i,s)} \vec{F}_n^{(i,s)} \\ \hat{Y}_i^{(s)} = \sum_{n=N_i^{(s)}+1}^{\infty} \left| \vec{F}_n^{(i,s)} \right\rangle Y_n^{(i,s)} \left\langle \vec{F}_n^{(i,s)} \right| \end{cases} \qquad (12)$$

where $I_n^{(i,s)} = I_n^{(i,s,A)} + I_n^{(i,s,B)}$ [with $n = 1, 2, \ldots, N_i^{(s)}$] is the amplitude of the n-th active mode in $D_i^{(s)}$ and $Y_n^{(i,s)} = Y_n^{(i,s,A)} + Y_n^{(i,s,B)}$ denotes the total modal admittance viewed by $D_i^{(s)}$. This expression is symbolized by the Norton generator shown in Figure 6(a).
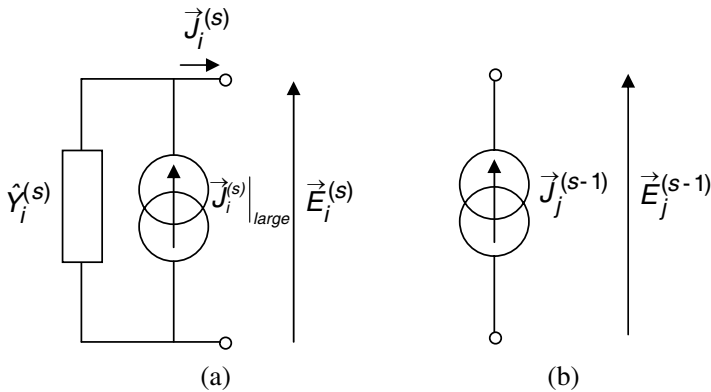

Figure 6. Symbolic representations of the current Scale Changing Sources: (a) In the domain $D_i^{(s)}$ (scale level s); (b) In the sub-domain $D_j^{(s-1)}$ (scale level $s-1$). These sources allow deriving impedance matrix characterizing the Scale-Changing Network that models the electromagnetic coupling between the scale s and the scale $s-1$.

2.4.2. Modal Scale-Changing Sources at the Smaller Scale

The *current* Scale-Changing source in the sub-domain $D_j^{(s-1)}$ (scale $s-1$) is defined as the linear combination of $N_j^{(s-1)}$ active modes as followed:

$$\vec{J}_j^{(s-1)} = \left. \vec{J}_j^{(s-1)} \right|_{large} = \sum_{n=1}^{N_j^{(s-1)}} I_n^{(j,s-1)} \vec{F}_n^{(j,s-1)} \tag{13}$$

where $I_n^{(j,s-1)} \vec{F}_n^{(j,s-1)}$ denotes the current density of the n-th active mode in the sub-domain $D_j^{(s-1)}$. Modelling the coupling between the scale s and scale $s-1$, the contribution $\left. \vec{J}_j^{(s-1)} \right|_{fine}$ of passive modes to the total current density $\vec{J}_j^{(s-1)}$ in $D_j^{(s-1)}$ does not act as an actual source. The symbolic representation of the current Scale Changing Source at scale $s-1$ is shown in Figure 6(b). At this smaller scale, the admittance operator that models the half-regions located on both sides of the discontinuity plane is not taken into consideration unlike at the
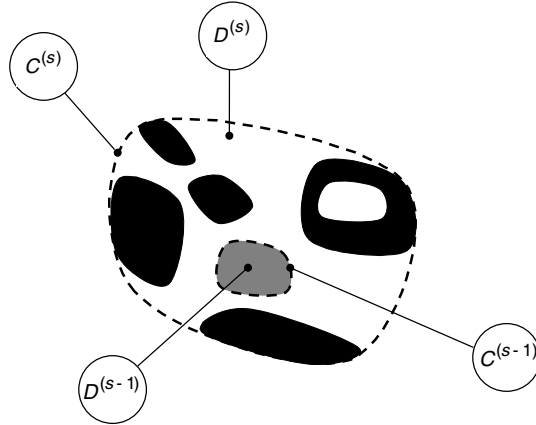
Figure 7. The generic domain $D^{(s)}$ (scale s) resulting from the partition process. Black is the sub-domain $D_{metal}^{(s)}$ of the perfect electric conductors; White is the sub-domain $D_{diel.}^{(s)}$ of the lossless dielectric and Grey indicates the sub-domain $D^{(s-1)}$ (scale $s-1$). The dotted line indicates the contour along which artificial boundary conditions are incorporated.

higher scale level s: this choice allows eliminating redundancies in the theoretical formulation when cascading of Scale-Changing Networks.

2.5. Derivation of the Scale-Changing Network

The objective of this section is to derive the SCN that models the electromagnetic coupling between two adjacent scale levels, that is, the coupling between active modes in the generic domain $D_i^{(s)}$ and its constitutive sub-domains $D_j^{(s-1)}(j = 1, 2, \ldots, J_{s-1})$.

2.5.1. Formulation of the Boundary Value Problem

For the sake of clarity in the theoretical developments, consider the domain $D^{(s)}$ composed of *one* sub-domain $D^{(s-1)}$ (see Figure 7).

The domain of perfectly conducting metallic patterns is denoted $D_{metal}^{(s)}$ while the domain $D_{diel.}^{(s)}$ designates the lossless dielectric region. The generalization of this problem to multiple sub-domains $D_j^{(s-1)}$ is straightforward and is not reported here. In order to derive the impedance matrix of the SCN that models the electromagnetic coupling between the scale s and $s - 1$, the current Scale-Changing Source shown in Figure 6(a) is incorporated in the domain $D^{(s)}$ while the current Scale-Changing Source shown in Figure 6(a) is inserted in the smaller domain $D^{(s-1)}$. The boundary conditions prescribed on the tangential components of the electromagnetic field in $D^{(s)} = D_{metal}^{(s)} \cup D_{diel.}^{(s)} \cup D^{(s-1)}$ are given by:

$$\vec{E}^{(s)} = \vec{E}_A^{(s)} = \vec{E}_B^{(s)} = \vec{0} \text{ in } D_{metal}^{(s)} \tag{14a}$$

$$\left. \begin{array}{l} \vec{E}^{(s)} = \vec{E}_A^{(s)} = \vec{E}_B^{(s)} \\ \vec{J}^{(s)} = \vec{H}_A^{(s)} \times \vec{n}_A + \vec{H}_B^{(s)} \times \vec{n}_B = \vec{0} \end{array} \right\} \text{ in } D_{diel.}^{(s)} \tag{14b}$$

$$\vec{J}^{(s-1)} = \sum_{n=1}^{N^{(s-1)}} I_n^{(s-1)} \vec{F}_n^{(s-1)} \text{ in } D^{(s-1)} \tag{14c}$$

where $I_n^{(s-1)}$ for $n = 1, 2, \ldots, N^{(s-1)}$ designates the current amplitude of the nth mode $\vec{F}_n^{(s-1)}$ in $D^{(s-1)}$. The quantity $N^{(s-1)}$ denotes the number of active modes in the domain $D^{(s-1)}$. The current Scale Changing Source at scale s (domain $D^{(s)}$) is defined by the Eqs. (10) and (12). The boundary conditions Eq. (14) may then be represented by the equivalent circuits shown in Figure 8. Each circuit represents the boundary conditions prescribed in a specific domain.
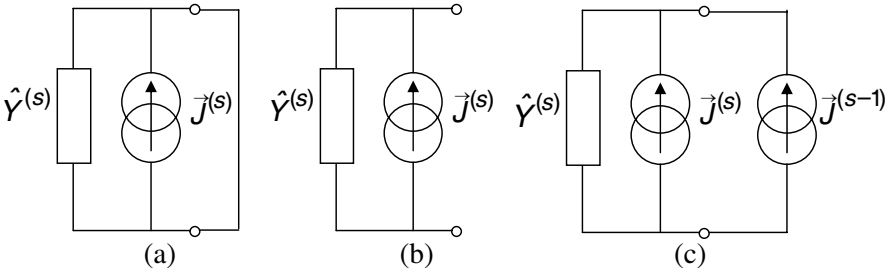
Figure 8. Equivalent circuits representing the boundary conditions in (a) the perfect electric conductors domain $D^{(s)}_{metal}$, (b) the lossless dielectric domain $D^{(s)}_{diel.}$ and (c) domain $D^{(s-1)}$.

It will be shown that all circuits of Figure 8 can be integrated into a single network by incorporating *virtual sources* in the domain $D^{(s)}$, that is, sources that do not supply electromagnetic power in this domain. The concept of virtual sources and its representation by an equivalent circuit have been proposed by H. Baudrand [20–23] as a very convenient way to derive the boundary value problem in term of an integral equation. It has been applied with success to the modelling of microwave circuits by taking into account the metallic losses (see, e.g., [24]). Define two virtual field sources $\vec{e}^{(s-1)}$ and $\vec{e}^{(s)}_{diel}$ respectively in the domains $D^{(s-1)}$ and $D^{(s)}_{diel.}$ (*Note*: a vector is *defined* in a domain D when it is non zero in D and zero outside D). Since the power supplied by the virtual sources in $D^{(s-1)}$ is zero by definition, the dual quantity $\vec{j}^{(s-1)}$ of the virtual source $\vec{e}^{(s-1)}$ is defined outside the domain $D^{(s-1)}$; moreover since the power supplied by the virtual sources in $D^{(s)}_{diel.}$ is zero by definition, the dual quantity $\vec{j}^{(s)}_{diel}$ of the virtual source $\vec{e}^{(s)}_{diel}$ is defined outside the domain $D^{(s)}_{diel.}$. Therefore:

$$\begin{cases} \vec{j}^{(s-1)} = \vec{0} & \text{in} \quad D^{(s-1)} \\ \vec{j}^{(s)}_{diel} = \vec{0} & \text{in} \quad D^{(s)}_{diel.} \end{cases} \tag{15}$$

The Figure 9 gives the equivalent network that represents the boundary conditions in the entire domain $D^{(s)}$. As illustrated in Figure 10 the network of Figure 9 is equivalent to one given in Figure 8(a) in domain $D^{(s)}_{metal}$, in Figure 8(b) in domain $D^{(s)}_{diel.}$, in Figure 8(c) in the sub-domain $D^{(s-1)}$.

From the Kirchhoff's and Ohm's laws, applied to the equivalent
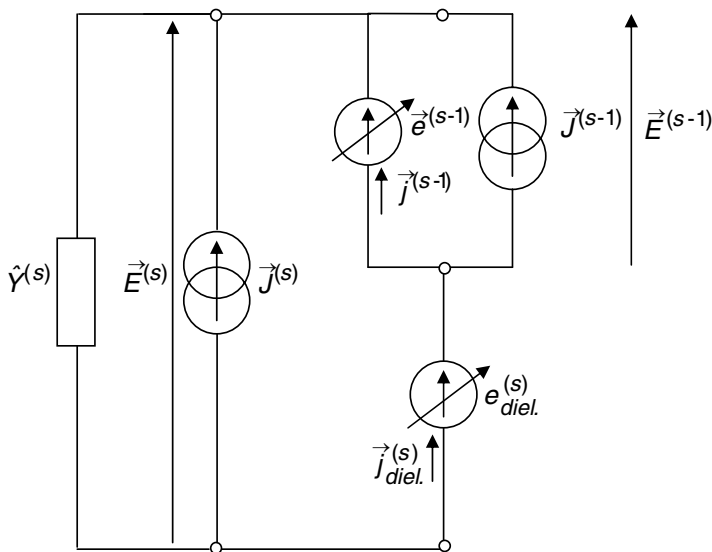
Figure 9. Equivalent network representation of the boundary value conditions in the domain $D^{(s)}$.

network of Figure 9 the relationship between the (virtual and Scale-Changing) sources and their dual quantities is derived:

$$
\underbrace{\begin{bmatrix} \vec{E}^{(s)} \\ \vec{E}^{(s-1)} \\ \vec{j}^{(s-1)} \\ j_{diel}^{(s)} \end{bmatrix}}_{\substack{\text{dual quantities} \\ \text{of the sources}}} = \begin{bmatrix} 0 & 0 & \hat{1} & \hat{1} \\ 0 & 0 & \hat{1} & 0 \\ -\hat{1} & -\hat{1} & \hat{Y}^{(s)} & \hat{Y}^{(s)} \\ -\hat{1} & 0 & \hat{Y}^{(s)} & \hat{Y}^{(s)} \end{bmatrix} \underbrace{\begin{bmatrix} \vec{J}^{(s)} \\ \vec{J}^{(s-1)} \\ \vec{e}^{(s-1)} \\ \vec{e}_{diel}^{(s)} \end{bmatrix}}_{\text{sources}} \tag{16}
$$

where $\hat{1} = \sum\limits_{n=N^{(s)}+1}^{\infty} \left| \vec{F}_n^{(s)} \right\rangle \left\langle \vec{F}_n^{(s)} \right|$ designates the identity operator in the domain $D^{(s)}$ [that is, $\hat{1}\vec{f} = \vec{f}$ for vector $\vec{f}$ defined in $D^{(s)}$] and from Eq. (12), the admittance operator $\hat{Y}^{(s)}$ is given by $\hat{Y}^{(s)} = \sum\limits_{n=N^{(s)}+1}^{\infty} \left| \vec{F}_n^{(s)} \right\rangle Y_n^{(s)} \left\langle \vec{F}_n^{(s)} \right|$ where $Y_n^{(s)}$ is the total modal admittance viewed by $D_i^{(s)}$. The formulation of the boundary value problem in the domain $D^{(s)}$ consists of combining Eq. (15) and Eq. (16).
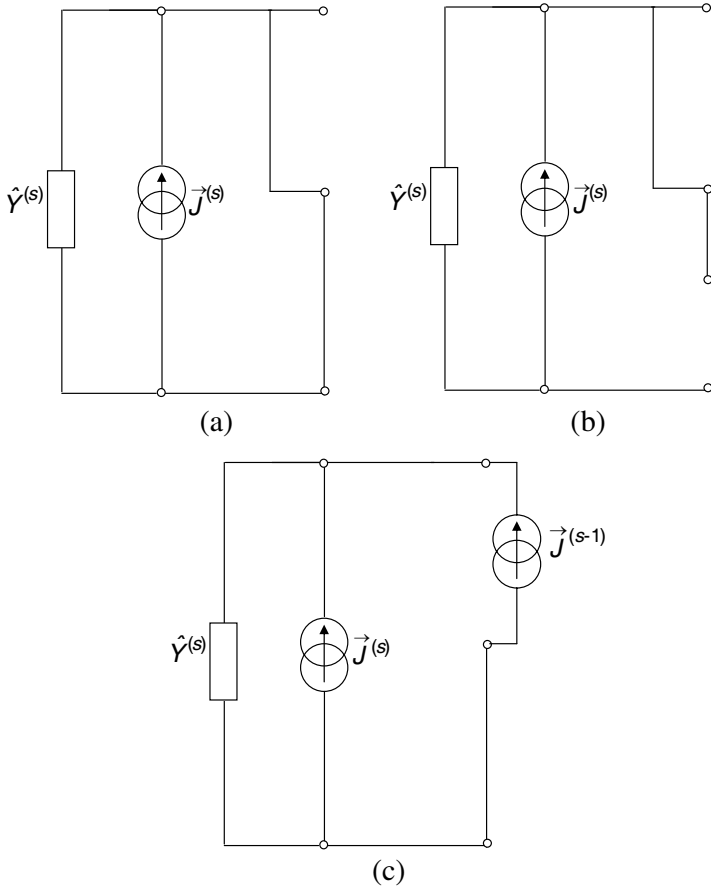
Figure 10. The network in Figure 9 is equivalent to one in: (a) Figure 8(a) in domain $D_{metal}^{(s)}$, (b) Figure 8(b) in domain $D_{diel.}^{(s)}$, (c) Figure 8(c) in the sub-domain $D^{(s-1)}$.

2.5.2. Numerical Resolution of the Boundary Value Problem

The resolution of the boundary value problem derived in Section 2.5.1 is performed by applying the Galerkin's method (see the Appendix). The Scale-Changing Network that models the electromagnetic coupling between the scale s and the scale $s-1$ is then found to be characterized by an impedance matrix $\left[Z^{(s,s-1)}\right]$, that is:

$$\left[V^{(s,s-1)}\right] = \left[Z^{(s,s-1)}\right]\left[I^{(s,s-1)}\right] \tag{17}$$
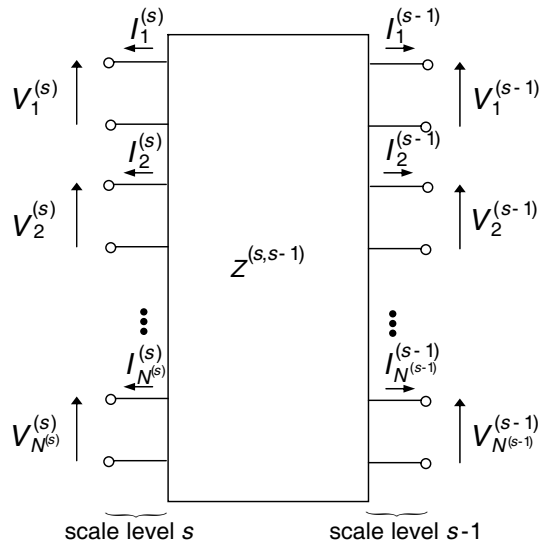
Figure 11. SCN modelling the coupling between scale s and scale $s - 1$ for a domain composed one sub-domain at scale $s - 1$.

where $\left[V^{(s,s-1)}\right] = \begin{bmatrix} \left[V^{(s)}\right] \\ \left[V^{(s-1)}\right] \end{bmatrix}$ and $\left[I^{(s,s-1)}\right] = \begin{bmatrix} \left[I^{(s)}\right] \\ \left[I^{(s-1)}\right] \end{bmatrix}$.

Moreover $\left[V^{(s)}\right]$ and $\left[I^{(s)}\right]$ are column vectors of the $N^{(s)}$ elements $V_n^{(s)}$ and $I_n^{(s)}$, respectively. The quantities $V_n^{(s)}$ and $I_n^{(s)}$ designate respectively the voltage and current amplitudes of the n-th mode in $D^{(s)}$ while $N^{(s)}$ is the number of active modes at scale s. Also, $\left[V^{(s-1)}\right]$ and $\left[I^{(s-1)}\right]$ are column vectors of the $N^{(s-1)}$ elements $V_n^{(s-1)}$ and $I_n^{(s-1)}$, respectively. The quantities $V_n^{(s-1)}$ and $I_n^{(s-1)}$ designate respectively the voltage and current amplitudes of the n-th mode in $D^{(s-1)}$ while $N^{(s)}$ is the number of active modes at scale s. The relationship of Eq. (17) is represented by the multi-port shown in Figure 11.

3. GLOBAL ELECTROMAGNETIC SIMULATION OF COMPLEX STRUCTURES VIA THE CASCADE OF SCALE-CHANGING NETWORKS

As discussed in Section 2.3, the electromagnetic modelling of multi-scale planar structures is performed by interconnecting Scale-Changing Networks, each network models the electromagnetic coupling

between two adjacent scales. The reduction of the electromagnetic modelling of complex structures to the cascade of Scale-Changing Networks (SCN) is called the *Scale-Changing Technique* (SCT). This monolithic (unique) approach for the global electromagnetic simulation of complex structures does not require delicate interconnection of heterogeneous theoretical formulations. Due to the hierarchical-domain decomposition provided by the partitioning process, the complex structures are broken down into a finite number of scale levels; next all the SCN that relate the electromagnetic field at adjacent scales are separately computed and, the hierarchical interconnection of the SCN is finally performed for global electromagnetic simulation of complex (multi-scale) structures. The scale crossing from the smallest to the arbitrary scale S is performed by shunting the cascade of SCN by the equivalent multi-ports modelling the smallest scale. When the dimensions of a sub-domain are small compared to the wavelength the corresponding multi-port reduces to one-port classically called *surface impedance*. However, for reaching the convergence of the numerical results, the larger the size of the sub-domain the higher the number of active and passive modes.

The SCN-based approach avoids the direct computation of structure with high aspect ratio and consequently, as far as the number of modes in the computation of SCN is not very large, it does thus not suffer from the treatment of ill-conditioned matrices and the lack of proper convergence. Typically, if N orders of magnitude (or decades) separate the largest to the smallest dimensions in the structure the SCN-based global electromagnetic simulation requires the computation of N SCN (or matrices), while tremendous execution time and memory resources are required by other numerical techniques for handling the corresponding aspect ratio of 10^N. Moreover, the SCN can be computed separately and consequently, the SCN-based numerical technique is highly parallelizable.

In the design and optimization processes modifications of the structure geometry may occur at a given scale S. Contrarily to classical meshing-based techniques, these modifications do not require the recalculation of the overall structure but only the SCN modeling the electromagnetic coupling between scale S and $S-1$ and, between $S+1$ and S. Such modularity makes the SCN-based approach very efficient in terms of CPU time and a very powerful analysis, design and optimization tool for engineers who design complex structures.

When dimensions of domains are large compared to the wavelength high-frequency techniques based on the asymptotic electromagnetic approaches (e.g., Physical Theory of Diffraction) must be preferred to the SCT and low-frequency techniques are also more

efficient than SCT at fine scale. However the SCT seems to be a good candidate to provide an efficient and powerful approach for bridging the gap between high- and low-frequency techniques, that is, between large- and small-scale electromagnetic modelling.

Illustration of all the above mentioned features and quantitative information about execution time in some specific cases may be found in the previous reports [6, 8]. These illustrations cover bounded and un-bounded structures. In particular it has been shown that the SCN-based approach can be advantageously applied to pre-fractal planar structures, that is, to complex structures presenting scale-invariance symmetry over a wide scale range. It consists of an alternative technique to the renormalization approach proposed by H. Baudrand et al. [26, 27]. The proposed technique reduces in these cases to simple recurrent relationships and allows a dramatic reduction in the computational time compared to classical numerical techniques, especially when the complexity — i.e., the number of scale levels — is high (see, e.g., [8]).

4. CONCLUSION

A monolithic formulation for the global electromagnetic simulation of multi-scale 2.5D structures has been presented. It consists of the cascade of *Scale-Changing Networks*, each network models the electromagnetic coupling between adjacent scale levels. By its very nature, this formulation is highly parallelizable, which also distinguishes it from other techniques that have to be adapted for distributed processing.

APPENDIX A.

The boundary value problem in the domain $D^{(s)}$ shown in Figure 7 is derived in Section 2.5.1. It can be written as followed:

$$\begin{cases} \vec{j}^{(s-1)} = \vec{0} \quad \text{in} \quad D^{(s-1)} \\ \vec{j}^{(s)}_{diel} = \vec{0} \quad \text{in} \quad D^{(s)}_{diel.} \end{cases} \tag{A1}$$

with

$$\begin{bmatrix} \vec{E}^{(s)} \\ \vec{E}^{(s-1)} \\ \vec{j}^{(s-1)} \\ j^{(s)}_{diel} \end{bmatrix} = \begin{bmatrix} 0 & 0 & \hat{1} & \hat{1} \\ 0 & 0 & \hat{1} & 0 \\ -\hat{1} & -\hat{1} & \hat{Y}^{(s)} & \hat{Y}^{(s)} \\ -\hat{1} & 0 & \hat{Y}^{(s)} & \hat{Y}^{(s)} \end{bmatrix} \begin{bmatrix} \vec{J}^{(s)} \\ \vec{J}^{(s-1)} \\ \vec{e}^{(s-1)} \\ \vec{e}^{(s)}_{diel} \end{bmatrix} \tag{A2}$$

This boundary value problem may be solved by applying the Galerkin's Method. Here it consists of expanding the unknown tangential electric field inside domains $D^{(s-1)}$ and $D^{(s)}_{diel.}$ on two normal sets of entire-domain trial functions, respectively (see, e.g., [25] for the use of entire-domain trial functions in the electromagnetic analysis of planar structures):

(1) Let $\left\{\vec{g}_m^{(s-1)}\right\}_{m=1,2,\ldots M_e^{(s-1)}}$ be a set of $M_e^{(s-1)}$ entire domain trial functions defined in $D^{(s-1)}$. The unknown tangential electric field $\vec{e}^{(s-1)}$ in this domain may be approximated by the following truncated series:

$$\vec{e}^{(s-1)} = \sum_{m=1}^{M_e^{(s-1)}} a_m^{(s-1)} \vec{g}_m^{(s-1)} \tag{A3}$$

with

$$\left\langle \vec{g}_m^{(s-1)}, \vec{g}_n^{(s-1)} \right\rangle = \iint\limits_{D^{(s)}} \left[\vec{g}_m^{(s-1)} \right]^* \cdot \vec{g}_n^{(s-1)} ds$$

$$= \iint\limits_{D^{(s-1)}} \left[\vec{g}_m^{(s-1)} \right]^* \cdot \vec{g}_n^{(s-1)} ds = \delta_{mn} \tag{A4}$$

and

$$a_m^{(s-1)} = \left\langle \vec{g}_m^{(s-1)}, \vec{e}^{(s-1)} \right\rangle \tag{A5}$$

By definition the current density $\vec{j}^{(s-1)}$ in domain $D^{(s-1)}$ is zero while the tangential electric field $\vec{e}^{(s-1)}$ and the trial functions $g_m^{(s-1)}$ for $m = 1, 2, \ldots, M_e^{(s-1)}$ are zero in the complementary domain $\bar{D}^{(s-1)}$ to $D^{(s)} = D^{(s-1)} \cup \bar{D}^{(s-1)}$. Consequently for $m = 1, 2, \ldots, M_e^{(s-1)}$:

$$\left\langle \vec{g}_m^{(s-1)}, \vec{j}^{(s-1)} \right\rangle = \iint\limits_{D^{(s)}} \left[\vec{g}_m^{(s-1)} \right]^* \cdot \vec{j}^{(s-1)} ds$$

$$= \iint\limits_{D^{(s-1)}} \left[\vec{g}_m^{(s-1)} \right]^* \cdot \vec{0} ds + \iint\limits_{\bar{D}^{(s-1)}} \vec{0} \cdot \vec{j}^{(s-1)} ds = 0 \tag{A6}$$

(2) Let $\left\{ \vec{h}_m^{(s)} \right\}_{m=1,2,\ldots,N_e^{(s)}}$ be a set of $N_e^{(s)}$ entire domain trial functions defined in $D^{(s)}_{diel.}$. The unknown tangential electric field

$\vec{e}_{diel}^{(s)}$ in this domain may be represented by the following truncated series:

$$\vec{e}_{diel}^{(s)} = \sum_{m=1}^{N_e^{(s)}} b_m^{(s)} \vec{h}_m^{(s)} \tag{A7}$$

with

$$\left\langle \vec{h}_m^{(s)}, \vec{h}_n^{(s)} \right\rangle = \iint\limits_{D^{(s)}} \left[\vec{h}_m^{(s)} \right]^* \cdot \vec{h}_n^{(s)} ds = \iint\limits_{D_{diel.}^{(s)}} \left[\vec{h}_m^{(s)} \right]^* \cdot \vec{h}_n^{(s)} ds = \delta_{mn} \tag{A8}$$

and

$$b_m^{(s)} = \left\langle \vec{h}_m^{(s)}, \vec{e}_{diel}^{(s)} \right\rangle \tag{A9}$$

By definition the current density $\vec{j}_{diel}^{(s)}$ in domain $D_{diel.}^{(s)}$ is zero while the tangential electric field $\vec{e}_{diel}^{(s)}$ and the trial functions $\vec{h}_m^{(s)}$ for $m = 1, 2, \ldots, N_e^{(s)}$ are zero in the complementary domain $\bar{D}_{diel.}^{(s)}$ to $D^{(s)} = D_{diel}^{(s)} \cup \bar{D}_{diel}^{(s)}$. Consequently, for $m = 1, 2, \ldots, N_e^{(s)}$:

$$\left\langle \vec{h}_m^{(s)}, \vec{j}_{diel}^{(s)} \right\rangle = \iint\limits_{D^{(s)}} \left[\vec{h}_m^{(s)} \right]^* \cdot \vec{j}_{diel}^{(s)} \, ds$$

$$= \iint\limits_{D_{diel}^{(s)}} \left[\vec{h}_m^{(s)} \right]^* \cdot \vec{0} \cdot ds + \iint\limits_{\bar{D}_{diel}^{(s)}} \vec{0} \cdot \vec{j}_{diel}^{(s)} \, ds = 0 \tag{A10}$$

Moreover, following Section 2.4.1, the tangential electric field $\vec{E}^{(s)}$ and the current density $\vec{J}^{(s)}$ inside the domain $D^{(s)}$ may be expanded on the discrete normal set of modes $\left\{ \vec{F}_n^{(s)} \right\}_{n=1,2,\ldots}$ in this domain, that is:

$$\vec{E}^{(s)} = \sum_{n=1}^{\infty} V_n^{(s)} \vec{F}_n^{(s)} \quad \text{and} \quad \vec{J}^{(s)} = \sum_{n=1}^{N^{(s)}} I_n^{(s)} \vec{F}_n^{(s)} \tag{A11}$$

With $\left\langle \vec{F}_m^{(s)}, \vec{F}_n^{(s)} \right\rangle = \iint\limits_{D^{(s)}} \left[\vec{F}_m^{(s)} \right]^* \cdot \vec{F}_n^{(s)} ds = \delta_{mn}$. In Eq. (A11) the quantities $V_n^{(s)}$ and $I_n^{(s)}$ designate respectively the voltage and current amplitudes of the n-th mode in $D^{(s)}$. Following Section 2.4.2, the tangential electric field $\vec{E}^{(s-1)}$ and the current density $\vec{J}^{(s-1)}$ inside

the domain $D^{(s-1)}$ may be expanded on the discrete normal set of modes $\left\{ \vec{F}_n^{(s-1)} \right\}_{n=1,2,\ldots}$ in this domain, that is:

$$\vec{E}^{(s-1)} = \sum_{n=1}^{N^{(s-1)}} V_n^{(s-1)} \vec{F}_n^{(s-1)} \text{ and } \vec{J}^{(s-1)} = \sum_{n=1}^{N^{(s-1)}} I_n^{(s-1)} \vec{F}_n^{(s-1)} \quad (A12)$$

with $\left\langle \vec{F}_m^{(s-1)}, \vec{F}_n^{(s-1)} \right\rangle = \iint\limits_{D^{(s-1)}} \left[\vec{F}_m^{(s-1)} \right]^* \cdot \vec{F}_n^{(s-1)} ds = \delta_{mn}$. In Eq. (A12) $V_n^{(s-1)}$ and $I_n^{(s-1)}$ designate respectively the voltage and current amplitudes of the n-th mode in $D^{(s-1)}$. By applying the Galerkin method to the boundary value problem the following linear system of equations is then derived:

$$
\begin{bmatrix} \left[V^{(s)} \right] \\ \left[V^{(s-1)} \right] \\ [0] \\ [0] \end{bmatrix}
$$
$$
= \begin{bmatrix} [0] & [0] & [P] & [Q] \\ [0] & [0] & [R] & [0] \\ -[P]^{*T} & -[R]^{*T} & \left[\hat{Y} \right]_{11} & \left[\hat{Y} \right]_{12} \\ -[Q]^{*T} & [0] & \left[\hat{Y} \right]_{21} & \left[\hat{Y} \right]_{22} \end{bmatrix} \begin{bmatrix} \left[I^{(s)} \right] \\ \left[I^{(s-1)} \right] \\ \left[a^{(s-1)} \right] \\ \left[a^{(s)} \right] \end{bmatrix} \quad (A13)
$$

where $\left[V^{(scale)} \right]$ and $\left[I^{(scale)} \right]$ (with scale $= s, s-1$) are column vectors of the $N^{(scale)}$ elements $V_n^{(scale)}$ and $I_n^{(scale)}$ respectively, $\left[a^{(s-1)} \right]$ is a column vector of $M_e^{(s-1)}$ elements $a_m^{(s-1)}$, $\left[a^{(s)} \right]$ is a column vector of $N_e^{(s)}$ elements $b_m^{(s)}$; $[P]$ is a $N^{(s)} \times M_e^{(s-1)}$ matrix of elements $\left\langle F_m^{(s)}, \vec{g}_n^{(s-1)} \right\rangle$, $[Q]$ is a $N^{(s)} \times N_e^{(s)}$ matrix of elements $\left\langle F_m^{(s)}, \vec{h}_n^{(s)} \right\rangle$, $[R]$ is a $N^{(s-1)} \times M_e^{(s-1)}$ matrix of elements $\left\langle F_m^{(s-1)}, \vec{g}_n^{(s-1)} \right\rangle$, $\left[\hat{Y} \right]_{11}$ is a $M_e^{(s-1)} \times M_e^{(s-1)}$ matrix of elements $\left\langle \vec{g}_m^{(s-1)}, \hat{Y}^{(s)} \vec{g}_n^{(s-1)} \right\rangle$, $\left[\hat{Y} \right]_{12}$ is a $M_e^{(s-1)} \times N_e^{(s)}$ matrix of elements $\left\langle \vec{g}_m^{(s-1)}, \hat{Y}^{(s)} \vec{h}_n^{(s)} \right\rangle$, $\left[\hat{Y} \right]_{21}$ is a $N_e^{(s)} \times M_e^{(s-1)}$ matrix of elements $\left\langle \vec{h}_m^{(s)}, \hat{Y}^{(s)} \vec{g}_n^{(s-1)} \right\rangle$ and finally $\left[\hat{Y} \right]_{22}$ is a $N_e^{(s)} \times N_e^{(s)}$ matrix of elements $\left\langle \vec{h}_m^{(s)}, \hat{Y}^{(s)} \vec{h}_n^{(s)} \right\rangle$. From Eq. (A13)

the unknown column vectors $\left[a^{(s-1)}\right]$ and $\left[a^{(s)}\right]$ may be expressed in the following form:

$$
\begin{bmatrix} \left[a^{(s-1)}\right] \\ \left[a^{(s)}\right] \end{bmatrix}
$$

$$
= \begin{bmatrix} \left[\hat{Y}\right]_{11} & \left[\hat{Y}\right]_{12} \\ \left[\hat{Y}\right]_{21} & \left[\hat{Y}\right]_{22} \end{bmatrix}^{-1} \begin{bmatrix} [P]^{*T} & [R]^{*T} \\ [Q]^{*T} & [0] \end{bmatrix} \begin{bmatrix} \left[I^{(s)}\right] \\ \left[I^{(s-1)}\right] \end{bmatrix} \quad \text{(A14)}
$$

Therefore:

$$
\left[\mathcal{V}^{(s,s-1)}\right] = [\mathcal{P}] \left[\hat{\mathcal{Y}}\right]^{-1} [\mathcal{P}]^{*T} \left[I^{(s,s-1)}\right] \quad \text{(A15)}
$$

with

$$
\left[\mathcal{V}^{(s,s-1)}\right] = \begin{bmatrix} \left[V^{(s)}\right] \\ \left[V^{(s-1)}\right] \end{bmatrix}, \left[I^{(s,s-1)}\right] = \begin{bmatrix} \left[I^{(s)}\right] \\ \left[I^{(s-1)}\right] \end{bmatrix}, \quad \text{(A16)}
$$

$$
[\mathcal{P}] = \begin{bmatrix} [P] & [Q] \\ [R] & [0] \end{bmatrix} \quad \text{(A17)}
$$

and

$$
[\hat{\mathcal{Y}}] = \begin{bmatrix} \left[\hat{Y}\right]_{11} & \left[\hat{Y}\right]_{12} \\ \left[\hat{Y}\right]_{21} & \left[\hat{Y}\right]_{22} \end{bmatrix} \quad \text{(A18)}
$$

REFERENCES

1. Mittra, R., J.-F. Ma, E. Lucente, and A. Monorhio, "CBMOM — An iteration free MoM approach for solving large multiscale EM radiation and scattering problems," *IEEE Antennas and Propagation Society International Symposium*, Vol. 2B, 2–5, Washington, D.C., Jul. 3–8, 2005.

2. Lucente, E., A. Monorchio, and R. Mittra, "Generation of characteristic basis functions by using sparse MoM impedance matrix to construct the solution of large scattering and radiation problems," *IEEE Antennas and Propagation Society International Symposium*, 4091–4094, Albuquerque, New Mexico, Jul. 9–14, 2006.

3. Nadarassin, M., H. Aubert, and H. Baudrand, "Analysis of planar structures by an integral multi-scale approach," *IEEE MTT-S International Microwave Symposium*, Vol. 2, 653–656, Orlando, Florida, USA, May 14–19, 1995.

4. Baudrand, H. and S. Wane, *Circuits Multi-échelles: Utilisation des Sources Auxiliaires. Modélisation Caractérisation et Mesures de Circuits Intégrés Passifs R.F*, Vol. 3, 75–108, Hermès, 2003.

5. Baudrand, H., "Electromagnetic study of coupling between active and passive circuits," *Microwave and Optoelectronics Conference*, Vol. 1, 143–152, Aug. 11–14, 1997.

6. Perret, E., H. Aubert, and H. Legay, "Scale-Changing technique for the electromagnetic modelling of MEMS-controlled planar phase-shifters," *IEEE Trans. Microwave Theory and Tech.*, Vol. 54, No. 9, 3594–3601, Sep. 2006.

7. Perret, E., N. Raveu, H. Aubert, and H. Legay, "Scale-Changing technique for MEMS-controlled phase-shifters," *36th European Microwave Week*, 866–869, Manchester, United Kingdom, Sep. 10–15, 2006.

8. Voyer, D., H. Aubert, and J. David, "Scale-changing technique for the electromagnetic modeling of planar self-similar structures," *IEEE Trans. Antennas Propagat.*, Vol. 54, No. 10, 2783–2789, Oct. 2006.

9. Voyer, D., H. Aubert, and J. David, "Radar cross section of discrete self-similar objects using a recursive electromagnetic analysis," *IEEE Antennas and Propagation Society International Symposium*, Vol. 4, 4260–4263, Monterey, California, USA, Jun. 20–26, 2004.

10. Voyer, D., H. Aubert, and J. David, "Radar cross section of self-similar targets," *Electronics Letters*, Vol. 41, No. 4, 215–217, Feb. 17, 2005.

11. Perret, E. and H. Aubert, "Scale-Changing technique for the computation of the input impedance of active patch antennas," *IEEE Antennas and Wireless Propagation Letters*, Vol. 4, 326–328, 2005.

12. Perret, E. and H. Aubert, "A multi-scale technique for the electromagnetic modeling of active antennas," *IEEE Antennas and Propagation Society International Symposium*, Vol. 4, 3923–3926, Monterey, California, USA, Jun. 20–25, 2004.

13. Raveu, N., G. Prigent, H. Aubert, P. Pons, and H. Legay, "Scale-Changing technique design and optimisation tool for active reflect-arrays cell," *37th European Microwave Conference*, 736–739, München, Germany, Oct. 9–12, 2007.

14. Nathalie Raveu, E. Perret, Hervé Aubert, and H. Legay, "Design of MEMS controlled phase shifter using SCT," *PIERS Online*, Vol. 3, No. 2, 230–232, Beijing, China, Mar. 26–30, 2007.

15. Raveu, N., E. Perret, H. Aubert, and H. Legay, "Scale-changing technique: A design tool for reflectarrays active cells," *Proceedings of the European Microwave Association*, Vol. 4, No. 2, 163–168, Journal of the European Microwave Association, Jun. 2008.

16. Collin, R. E., *Field Theory of Guided Waves*, 2nd edition, IEEE Press, 1991.

17. Rozzi, T. E. and W. F. G. Mecklenbräuker, "Wide-band network modelling of interacting inductive irises and steps," *IEEE Trans. Microwave Theory and Tech.*, Vol. 23, No. 2, 235–245, Feb. 1975.

18. Tao, J. W. and H. Baudrand, "Multimodal variational analysis of uniaxial waveguide discontinuities," *IEEE Trans. Microwave Theory and Tech.*, Vol. 39, No. 3, 506–516, Mar. 1991.

19. Chew, W. C., *Waves and Fileds in Inhomogeneous Media*, IEEE Press, 1995.

20. Baudrand, H., "Representation by equivalent circuit of the integral methods in microwave passive elements," *European Microwave Conference*, Vol. 2, 1359–1364, Budapest, Hungary, Sep. 10–13, 1990.

21. Baudrand, H., H. Aubert, D. Bajon, and F. Bouzidi, "Equivalent network representation of boundary conditions involving generalized trial quantities," *Annals of Telecommunications*, Vol. 52, No. 5–6, 285–292, 1997.

22. Baudrand, H., *Introduction au Calcul des Éléments de Circuits Passifs en Hyperfréquences*, Editions Cepadues, 2000.

23. Aubert, H. and H. Baudrand, *L'électromagnétisme par les Schémas Équivalents*, Editions Cepadues, 2003.

24. Bouzidi, F., H. Aubert, D. Bajon, and H. Baudrand, "Equivalent network representation of boundary conditions involving generalized trial quantities — Application to lossy transmission lines with finite metallization thickness," *IEEE Trans. Microwave Theory and Tech.*, Vol. 45, 869–876, Jun. 1997.

25. Nadarassin, M., H. Aubert, and H. Baudrand, "Analysis of planar structures by an integral approach using entire domain trial functions," *IEEE Trans. Microwave Theory and Tech.*, Vol. 10, 2492–2495, Oct. 1995.

26. Larbi, C., A. Bouallegue, and H. Baudrand, "Utilisation d'un processus de renormalisation pour l'étude électromagnétique des structures fractales bidimensionnelles," *Annales des Télécommunications*, Vol. 60, No. 7–8, 1023–1050, Juillet-Août, 2005.

27. Larbi, C., T. Ben Salah, T. Aguili, A. Bouallegue, and

H. Baudrand, "Study of the Sierpinski's Carpet fractal planar antenna by the renormalisation method," *International Journal of Microwave and Optical Technology*, 58–65, 2005.